

MAGNETIC ENERGY PRODUCTION BY TURBULENCE IN BINARY NEUTRON STAR MERGERS

JONATHAN ZRAKE AND ANDREW I. MACFADYEN

Center for Cosmology and Particle Physics, Physics Department, New York University, New York, NY 10003, USA
Draft version September 19, 2018

ABSTRACT

The simultaneous detection of electromagnetic and gravitational wave emission from merging neutron star binaries would aid greatly in their discovery and interpretation. By studying turbulent amplification of magnetic fields in local high-resolution simulations of neutron star merger conditions, we demonstrate that magnetar-level ($\gtrsim 10^{16}$ G) fields are present throughout the merger duration. We find that the small-scale turbulent dynamo converts 60% of the randomized kinetic energy into magnetic fields on a merger time scale. Since turbulent magnetic energy dissipates through reconnection events which accelerate relativistic electrons, turbulence may facilitate the conversion of orbital kinetic energy into radiation. If 10^{-4} of the $\sim 10^{53}$ erg of orbital kinetic available gets processed through reconnection, and creates radiation in the 15-150 keV band, then the fluence at 200 Mpc would be 10^{-7} erg/cm², potentially rendering most merging neutron stars in the advanced LIGO and Virgo detection volumes detectable by *Swift* BAT.

Subject headings: magnetohydrodynamics — turbulence — stars: neutron — magnetic fields — hydrodynamics — gamma-rays: bursts — X-rays: general — gravitational waves

1. INTRODUCTION

The in-spiral and coalescence of binary neutron star systems is a topic of increasingly intensive research in observational and theoretical astrophysics. It is anticipated that the first direct detections of gravitational wave (GW) will be from compact binary mergers. Binary neutron star (BNS) mergers are also thought to produce short-hard gamma-ray bursts (SGRB's) (Eichler et al. 1989; Narayan et al. 1992; Belczynski et al. 2006; Metzger et al. 2008). Simultaneous detections of a prompt gravitational wave signal with a spatially coincident electromagnetic (EM) counterpart dramatically increases the potential science return of the discovery. For this reason, there has been considerable interest as to which, if any, detectable EM signature may result from the merger (Metzger & Berger 2012; Piran et al. 2013). Other than SGRBs and their afterglows, including those viewed off-axis (Rhoads 1997; van Eerten & MacFadyen 2011), suggestions include optical afterglows associated with the radio-active decay of tidally expelled r-process material (Li & Paczyński 1998; Metzger et al. 2010) (though detailed calculations indicate they are faint (Barnes & Kasen 2013)), radio afterglows following the interaction of a mildly relativistic shell with the interstellar medium (Nakar & Piran 2011), and high-energy pre-merger emission from resistive magnetosphere interactions (Hansen & Lyutikov 2001; Piro 2012).

Merging neutron stars possess abundant orbital kinetic energy ($\sim 10^{53}$ ergs). A fraction of this energy is certain to be channelled through a turbulent cascade triggered by hydrodynamical instabilities during merger. Turbulence is known to amplify magnetic fields by stretching and folding embedded field lines in a process known as the small-scale turbulent dynamo (Vainshtein & Zel'dovich 1972; Chertkov et al. 1999; Tobias et al. 2011; Beresnyak 2012). Amplification stops when the magnetic energy grows to equipartition with the energy containing turbulent eddies (Schekochihin

et al. 2002, 2004; Federrath et al. 2011). An order of magnitude estimate of the magnetic energy available at saturation of the dynamo can be informed by global merger simulations. These studies indicate the presence of turbulence following the nonlinear saturation of the Kelvin-Helmholtz (KH) instability activated by shearing at the NS surface layers (Price & Rosswog 2006; Liu et al. 2008; Anderson et al. 2008; Rezzolla et al. 2011; Giacomazzo et al. 2011). The largest eddies produced are on the ~ 1 km scale and rotate at $\sim 0.1c$, setting the cascade time t_{eddy} and kinetic energy injection rate $\varepsilon_K \equiv E_K/t_{\text{eddy}}$ at 0.1ms and 5×10^{50} erg/s respectively. When kinetic equipartition is reached, each turbulent eddy contains 5×10^{46} erg of magnetic energy, and a mean magnetic field strength

$$B_{\text{RMS}} \gtrsim 10^{16} \text{G} \left(\frac{\rho}{10^{13} \text{g/cm}^3} \right)^{1/2} \left(\frac{v_{\text{eddy}}}{0.1c} \right). \quad (1)$$

Whether such conditions are realized in merging neutron star systems depends upon the dynamo saturation time t_{sat} and equipartition level E_{sat}/E_K . In particular, if $t_{\text{sat}} \lesssim t_{\text{merge}}$ then turbulent volumes of neutron star material will contain magnetar-level fields throughout the early merger phase. Once saturation is reached, a substantial fraction of the injected kinetic energy, $0.7\varepsilon_K$, is resistively dissipated (Haugen et al. 2004) at small scales. Magnetic energy dissipated by reconnection in optically thin surface layers will accelerate relativistic electrons (Blandford & Eichler 1987; Lyutikov & Uzdensky 2003), potentially yielding an observable electromagnetic counterpart, independently of whether the merger eventually forms a relativistic outflow capable of powering a short gamma-ray burst.

In this Letter we demonstrate that the small-scale turbulent dynamo saturates quickly, on a time $t_{\text{sat}} \lesssim t_{\text{merge}}$, and that $\gtrsim 10^{16}$ G magnetic fields are present throughout the early merger phase. This implies that the magnetic energy budget of merging binary neutron stars is

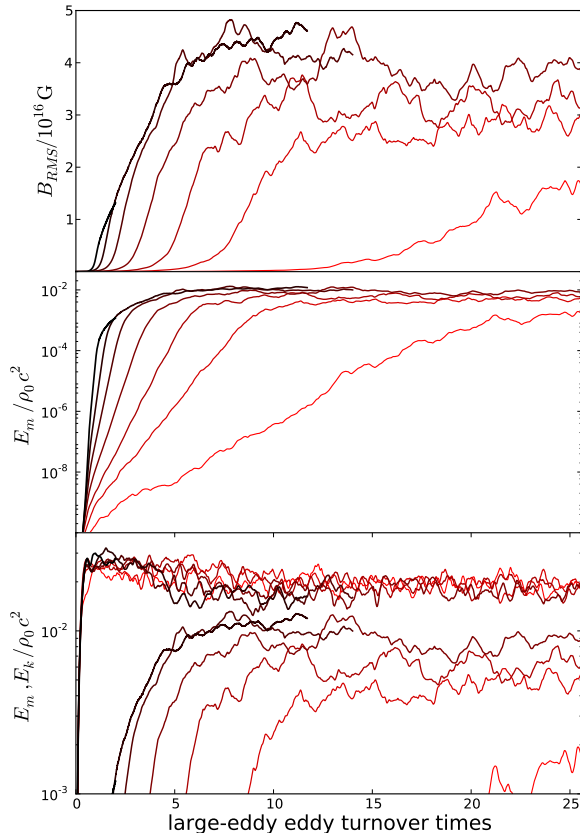


Figure 1. Time development of volume-averaged kinetic and magnetic energies at resolutions between 16^3 and 1024^3 . Lower resolutions are shown in red and graduate to black with higher resolution. *Top:* The root mean square magnetic field strength in units of 10^{16} G. When a turbulent volume is resolved by 16^3 zones, the small-scale dynamo proceeds so slowly that almost no amplification is observed in the first 1ms. *Middle:* The magnetic energy in units of the rest mass $\rho_0 c^2$ shown on logarithmic axes. It is clear that the linear growth rate increases at each resolution. *Bottom:* The kinetic energy (upper curves) shown again the magnetic energy (lower curves) again in units of $\rho_0 c^2$. For all resolutions, the kinetic energy saturates in less than $1 t_{\text{eddy}}$.

controlled by the rate with which hydrodynamical instabilities randomize the orbital kinetic energy. Our results are derived from simulations of the small scale turbulent dynamo operating in the high-density, trans-relativistic, and highly conductive material present in merging neutron stars. We have carefully examined the approach to numerical convergence and report grid resolution criteria sufficient to resolve aspects of the small-scale dynamo. Our Letter is organized as follows. The numerical setup is briefly described in Section 2. Section 3 reports the resolution criterion for numerical convergence of the dynamo completion time and the saturated field strength. In Section 4 we assess the possibility that magnetic reconnection events may convert a sufficiently large fraction of the magnetic energy into high energy photons to yield a prompt electromagnetic counterpart detectable by high energy observatories including *Swift* and *Fermi*.

2. NUMERICAL SCHEME AND PHYSICAL SETUP

The equations of ideal relativistic magnetohydrodynamics (RMHD) have been solved on the periodic unit cube with resolutions between 16^3 and 1024^3 .

$$\nabla_\nu N^\nu = 0 \quad (2a)$$

$$\nabla_\nu T^{\mu\nu} = S^\mu \quad (2b)$$

$$\frac{\partial \mathbf{B}}{\partial t} = \nabla \times (\mathbf{v} \times \mathbf{B}) \quad (2c)$$

Here, $b^\mu = F^\mu_\nu u^\nu$ is the magnetic field four-vector, and $h^* = 1 + e^* + p^*/\rho$ is the total specific enthalpy, where $p^* = p_g + b^2/2$ is the total pressure, p_g is the gas pressure and $e^* = e + b^2/2\rho$ is the specific internal energy. The source term $S^\mu = \rho a^\mu - \rho(T/T_0)^4 u^\mu$ includes injection of energy and momentum at the large scales and the subtraction of internal energy (with parameter $T_0 = 40\text{MeV}$) to permit stationary evolution. Vortical modes at $k/2\pi \leq 3$ are forced by the four-acceleration field $a^\mu = \frac{du^\mu}{d\tau}$ which smoothly decorrelates over a large-eddy turnover time, as described in Zrake & MacFadyen (2012, 2013).

We have employed a realistic micro-physical equation of state (EOS) appropriate for the conditions of merging neutron stars. It includes contributions from high-density nucleons according a relativistic mean field model (Shen et al. 1998; Shen et al. 2010), a relativistic and degenerate electron-positron component, neutrino and anti-neutrino pairs in beta equilibrium with the nucleons, and radiation pressure. For our conditions, all the components make comparable contributions to the pressure. We have also employed a simpler gamma-law EOS and found close agreement for the conditions explored in this paper, indicating that the MHD effects are insensitive the EOS for trans-sonic conditions. The models presented in our resolution study use the far less expensive gamma-law equation of state.

All of the simulations presented in this study use the HLLD approximate Riemann solver (Mignone et al. 2009), which has been demonstrated as crucial in providing the correct spatial distribution of magnetic energy in MHD turbulence (Beckwith & Stone 2011). The solution is advanced with an unsplit, second-order MUSCL-Hancock scheme. Spatial reconstruction is accomplished with the piecewise linear method configured to yield the smallest possible degree of numerical dissipation. The divergence constraint on the magnetic field is maintained to machine precision at cell corners using the finite volume CT method of Tóth (2002). Full details of the numerical scheme may be found in Zrake & MacFadyen (2012).

3. RESULTS

3.1. Growth and saturation of the magnetic energy

Magnetic fields are amplified in our simulations by the small-scale turbulent dynamo. Turbulent fluid motions stretch and fold the magnetic field lines, causing exponential growth of magnetic energy (e.g. Moffatt 1978). This growth is attributed to the advection and diffusion of \mathbf{B} through the MHD induction equation (Eq. 2c). When the magnetic field is weak ($E_M \ll E_K$) \mathbf{B} evolves passively, and the turbulence is hydrodynamical. This limit is referred to as small-scale kinematic turbulent dynamo, and is well described by Kazentzev's model

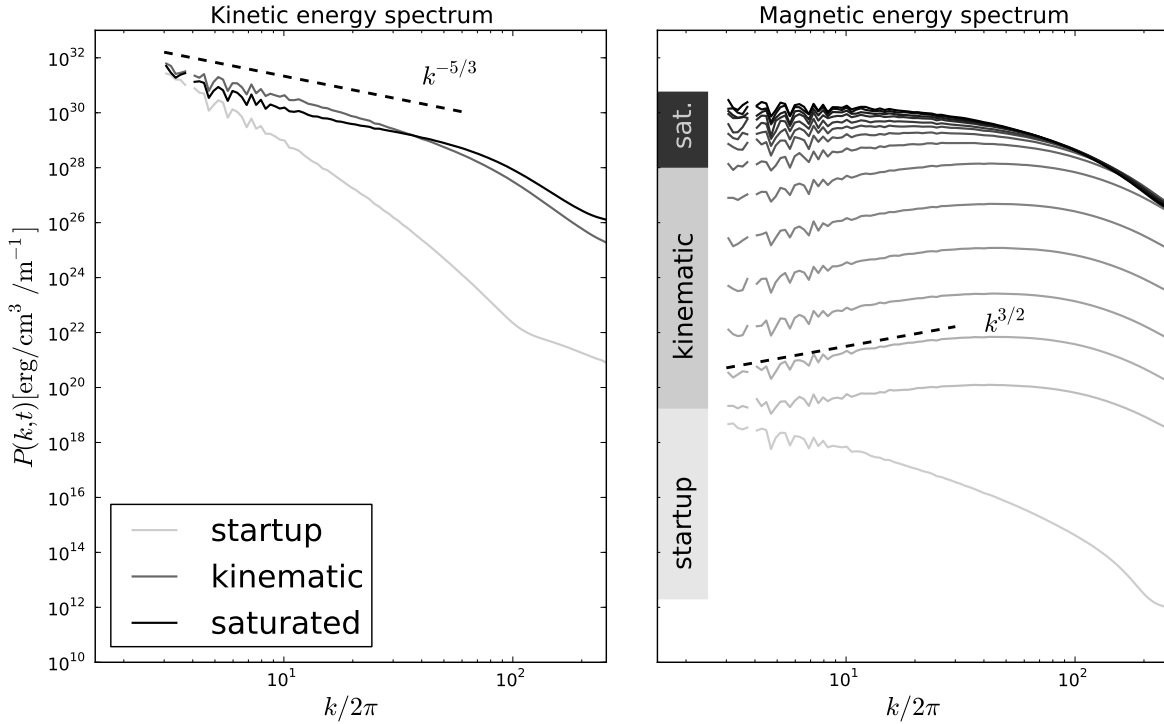


Figure 2. Time development of the spectrum of kinetic (left) and magnetic (right) energy, given in $\text{erg}/\text{cm}^3/\text{m}^{-1}$ for resolution 512^3 . During the *startup* phase the hydrodynamic cascade is not yet fully developed, this phase lasts for $1t_{\text{eddy}}$. The *kinematic* phase refers to the time when the hydrodynamic cascade is fully developed, but the magnetic energy is still energetically sub-dominant. During the *kinematic* phase, the kinetic energy power spectrum is consistent with a Kolmogorov cascade, having a slope $k^{-5/3}$ over intermediate wavelengths. Meanwhile, the magnetic energy spectrum is consistent with the Kazantsev description, having a positive slope $k^{3/2}$ over the same intermediate wavelengths. During this phase the magnetic energy exponentiates rapidly, with an e-folding time controlled by shearing at the smallest available scales. After *saturation*, the magnetic energy spectrum conforms to the kinetic energy spectrum, such that $E_M(k) \approx 4E_K(k)$ over the intermediate wavelengths. The kinetic energy spectrum after the dynamo completion has a slightly shallower slope than during the kinematic phase, but is still consistent with a $5/3$ spectral index.

(Kazantsev 1968). This model predicts that the power spectrum of magnetic energy peaks at the resistive scale ℓ_η and obeys a power law $k^{3/2}$ at longer wavelengths. The kinematic phase ends when the magnetic field acquires sufficient tension to modify the hydrodynamic motions, after which time a dynamical balance between kinetic and magnetic energy is established.

Numerical simulations of MHD turbulence are typically limited to magnetic Prandtl numbers $Pm \equiv \nu/\eta \approx 1$. However, neutron star material is characterized by $Pm \gg 1$, with the viscous cutoff due to neutrino diffusion occurring at around 10 cm, while the resistive scale is significantly smaller (Thompson & Duncan 1993). However, the disparity between true and simulated magnetic Prandtl number does not influence our conclusions. This is because dynamos are generically easier to establish in the high Pm regime than the small (Haugen et al. 2004; Ponty & Plunian 2011).

We use an initially uniform, pulsar-level (10^{11}G) seed magnetic field. This field is sub-dominant to the kinetic energy by 10 orders of magnitude, so that the initial field amplification is expected to be well-described by Kazantsev’s model. Indeed, we find that during this phase the power spectrum of magnetic energy follows $k^{3/2}$ (Fig. 2), peaking at around 10 grid zones, which

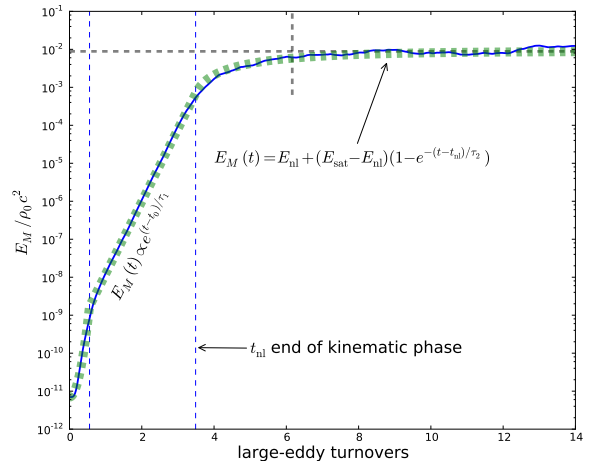


Figure 3. Time history of the magnetic energy for a representative run at 128^3 , together with the empirical model (Equation 3) with best-fit parameters. The horizontal dashed line indicates the magnetic energy, E_{sat} at the dynamo completion. From left to right, the vertical dashed lines mark the end of the startup, kinematic, and saturation phases.

we identify as the effective scale of resistivity. The saturation process begins at ever-earlier times with increasing numerical resolution. This reflects the fact that during the kinematic phase, magnetic energy exponentiates on a time scale controlled by shearing at the smallest scales. In numerically converged runs, full saturation occurs with $E_M \approx 0.6E_K$ and is characterized by scale-by-scale super-equipartition, with $E_K \approx 4E_M$ at all but the largest scale.

3.2. Numerical convergence

The same driven turbulence model was run through magnetic saturation at resolutions 16^3 , 32^3 , 64^3 , 128^3 , 256^3 , and 512^3 . Another model at 1024^3 was run through the end of the kinematic phase, but further evolution was computationally prohibitive. Fig. 1 shows the development of B_{RMS} , E_M , and E_K as a function of time at each resolution.

We find that sufficiently resolved runs ($\geq 512^3$) attain *mean* magnetic field strengths of 10^{16} G within two large eddy rotations. All models with resolutions $\geq 32^3$ eventually attain mean fields of $\gtrsim 3 \times 10^{16}$ G. The saturated field strength increases until resolution 256^3 . We find that the kinematic growth rate is higher at each higher resolution, while the time-scale for the non-linear saturation converges at 256^3 to roughly five large-eddy rotation times, or about 0.5ms for the physical parameters of binary neutron star mergers.

In order to quantitatively describe the time development of magnetic energy $E_M(t)$, we describe it with an empirical model,

$$E_M(t) = \begin{cases} E_M(0)e^{t^2/\tau_0^2} & 0 < t < t_1 \\ E_M(t_1)e^{-(t-t_1)/\tau_1} & t_1 < t < t_{nl} \\ E_{nl} + (E_{sat} - E_{nl})(1 - e^{-(t-t_{nl})/\tau_2}) & t_{nl} < t < \infty \end{cases} \quad (3)$$

where the 6 parameters (summarized in Table 1) are obtained by a least-squares optimization. Fig. 3 shows the empirical model given in Equation 3 applied to a representative run at 128^3 . The first phase, $t < t_1$ is a startup transient, and lasts until the hydrodynamic cascade is fully developed at $t_1 \approx t_{eddy}$. The kinematic dynamo phase lasts between t_1 and t_{nl} , during which the magnetic energy exponentiates on the time scale τ_1 . At t_{nl} , the smallest scales reach kinetic equipartition and the growth rate slows. In the final stage, E_M asymptotically approaches E_{sat} on the time-scale τ_2 . We define the dynamo completion time t_{sat} as $t_{nl} + \tau_2$. Fig. 4 shows the best-fit E_{sat} , t_{sat} , and τ_1 as a function of the resolution.

The magnetic energy E_{sat} at dynamo completion shows signs of converging to a value of $0.6E_K$ by resolution 512^3 . The time scale τ_2 on which the magnetic energy asymptotically approaches E_{sat} is consistently $\approx 3t_{eddy}$ at different resolutions. The dynamo completion time t_{sat} is numerically converged at $\approx 5t_{eddy}$ by 256^3 . The best-fit kinematic growth time follows a power law in the resolution, $\tau_1 \propto N^{-0.6}$. This is consistent with the value of $-2/3$ expected if the dynamo time is controlled by shearing at the smallest scale, the cascade is Kolmogorov (i.e. $u_\ell \propto \ell^{1/3}$), and the viscous cutoff ℓ_ν occurs at a fixed number of grid zones. In that case, $\tau_1 \sim t_\nu \propto \ell_\nu^{2/3} \sim N^{-2/3}$.

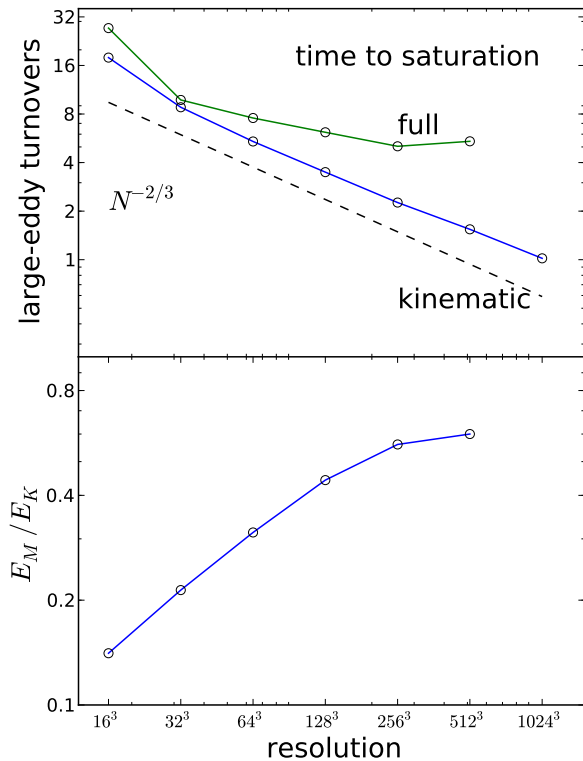


Figure 4. *Top:* Convergence study of the kinematic dynamo growth time τ_1 (blue) and the dynamo completion time t_{sat} (green) defined as $t_{nl} + \tau_2$. *Bottom:* Convergence study of the best-fit model parameter E_{sat} expressed as the ratio of magnetic to kinetic energy E_M/E_K . The converged value of the volume-averaged $E_M/E_K \approx 0.6$. Nevertheless, at intermediate wavelengths $E_M(k)/E_K(k) \approx 4$. As shown in Figure 2, the largest scales remain kinetically dominated. This indicates the suppression of coherent magnetic structure formation near the integral scale of turbulence.

3.3. Power spectrum of kinetic and magnetic energy

The time development of kinetic and magnetic energy power spectra has been studied for a single run with resolution 512^3 . We present three-dimensional, spherically integrated power spectra with the dimensions of $\text{ergs/cm}^3/\text{m}^{-1}$, defined as

$$P_K(k_i) = \frac{1}{\Delta k_i} \sum_{\mathbf{k} \in \Delta k_i} \left| \mathcal{F}_{\mathbf{k}} \left[\mathbf{v} \sqrt{\rho/2} \right] \right|^2 \quad (4a)$$

$$P_M(k_i) = \frac{1}{\Delta k_i} \sum_{\mathbf{k} \in \Delta k_i} \left| \mathcal{F}_{\mathbf{k}} \left[\mathbf{B} / \sqrt{8\pi} \right] \right|^2 \quad (4b)$$

where the Newtonian versions of kinetic and magnetic energy are appropriate since the conditions are only mildly relativistic. The definitions in Equations 4 satisfy $\int P(k) dk = \langle E \rangle$ for P_K and P_M . Figure 2 shows the power spectrum of kinetic and magnetic energy at various times throughout the growth and saturation of magnetic field. During the kinematic phase, the kinetic energy has a power spectrum $P_K(k) \propto k^{-5/3}$ consistent with the Kolmogorov theory for incompressible hydrodynamical turbulence, while $P_M(k, t) \propto e^{t/\tau_1} k^{3/2}$ consistent with Kazenstev's model. $P_M(k)$ maintains the same

Table 1
Empirical model for magnetic energy growth

Fit parameter	Description	Numerically converged value
τ_0	Startup time-scale	none, artifact
t_1	Hydrodynamic cascade fully developed	t_{eddy}
τ_1	Kinematic growth time-scale	none, $\propto N^{-2/3}$
t_{nl}	End of kinematic phase	$2t_{\text{eddy}}$
τ_2	Non-linear saturation time-scale	$t_{\text{nl}} + \tau_2 \approx 5t_{\text{eddy}}, 256^3$
E_{sat}	Saturated magnetic energy	$0.6E_K, 512^3$

Note. — Model parameters characterizing the growth of magnetic energy before and during the dynamo saturation. Numerical convergence is attained for the fully saturated magnetic energy E_{sat} and the dynamo completion time t_{sat} defined as $t_{\text{nl}} + \tau_2$.

shape, but exponentiates in amplitude at the time scale τ_1 which is controlled by shearing at the resistive scale. According to Kazentsev’s model, $P_M(k)$ should peak at the resistive scale. This is consistent with the observed peak in the magnetic energy at roughly 10 grid zones, the same scale at which we observe the viscous cutoff. This is also consistent with $\text{Pm} = 1$ expected from the numerical scheme employed.

When the magnetic energy at the resistive scale surpasses the level of the kinetic energy at that scale, $P_M(k)$ changes shape. The equipartition scale $\ell_{K,M}$ moves into the inertial range, and migrates to larger scale until full saturation occurs with $\ell_{K,M} \approx L/4$. The movement of $\ell_{K,M}$ to larger scale is associated with the formation of coherent and dynamically substantial magnetic structures of increasing size. The time-dependence has been suggested to be $\ell_{K,M} \propto t^{3/2}$ (Beresnyak et al. 2009). In the fully saturated state, the magnetic field is in scale-by-scale super-kinetic equipartition throughout the inertial range, with $P_M(k) \approx 4P_K(k)$. The largest scales remain kinetically dominated so that the numerically converged saturation level is $E_M \approx 0.6E_K$.

4. DISCUSSION

In this Letter we have determined the time scale and saturation level of the small-scale turbulent dynamo operating in the conditions of binary neutron star mergers. We have presented numerically converged simulations showing that magnetic fields are amplified to the $\sim 10^{16}\text{G}$ level within a small fraction of the merger dynamical time ($t_{\text{sat}} \lesssim t_{\text{merge}}$), independently of the seed field strength. If hydrodynamical instabilities create fluctuating velocities on the order of $0.1c$ as indicated by global simulations, then each 1km^3 turbulent volume dissipates $\gtrsim 10^{46}$ erg of magnetic energy per 0.1 ms. If f_{turb} represents the fraction of the merger remnant that contains such turbulence, the magnetic energy dissipated during the merger is at least

$$E_{\text{diss}} \sim 10^{49}\text{erg} \times \left(\frac{f_{\text{turb}}}{10^{-2}}\right) \left(\frac{t_{\text{merge}}}{1\text{ms}}\right) \quad (5)$$

A fraction of that dissipation will occur through magnetic reconnection in optically thin surface layers, supplying relativistic electrons which synchrotron radiate in the merger remnant magnetosphere. If 5% of that magnetic energy dissipation creates radiation in the 15–150 keV band, then the fluence at 200 Mpc would be $10^{-7}\text{erg}/\text{cm}^2$, potentially rendering most merging neutron stars in the advanced LIGO and Virgo detection volumes detectable by *Swift* BAT. If so, then merging neu-

tron stars are accompanied by a prompt electromagnetic counterpart, independently of whether a later merger phase yields a collimated outflow capable of powering a short gamma-ray burst.

We suggest that merger flares may be present in the current sample of short GRBs and may be roughly isotropic on the sky since they are seen to distances where the cosmological matter distribution becomes homogeneous. Searches for merger flares should seek to identify short flares, not unlike soft-gamma repeaters, among the short burst population. If mergers also produce short GRBs short-hard GRBs, then merger flares may constitute a precursor component of the emission.

The presence of strong magnetic fields may also aid in the ejection of neutron-rich material from surface layers of the merger remnant, possibly enhancing the enrichment of inter-stellar medium by r-process nuclei (Freiburghaus et al. 1999; Rosswog et al. 1999). Enhanced production of r-process nuclei also increases the likelihood of EM detection by radio-active decay powered afterglows, or “kilonovae” (Li & Paczyński 1998; Metzger et al. 2010).

Finally, it has been shown that magnetic fields will significantly influence the gravitational wave signature and remnant disk mass, if they exist at the 10^{17}G level (Etienne et al. 2012). Such strong fields are unlikely in older neutron star binaries, but our results suggest they may be revived, albeit at small scales, during the merger. To have significant influence, those fields would have to fill a considerable fraction of the merger volume. As we have shown in this Letter, the overall magnetic energy budget is controlled by the prevalence (f_{turb}) and vigor (ε_K) of the turbulent volumes. This fact motivates the use of higher resolution global simulations aimed at measuring f_{turb} and ε_K .

This research was supported in part by the NSF through grant AST-1009863 and by NASA through grant NNX10AF62G issued through the Astrophysics Theory Program. Resources supporting this work were provided by the NASA High-End Computing (HEC) Program through the NASA Advanced Supercomputing (NAS) Division at Ames Research Center.

REFERENCES

- Anderson, M., Hirschmann, E. W., Lehner, L., et al. 2008, *Phys Rev Lett*, 100, 191101
- Barnes, J., & Kasen, D. 2013, in *American Astronomical Society Meeting Abstracts*, Vol. 221, American Astronomical Society Meeting Abstracts, 346.04

- Beckwith, K., & Stone, J. M. 2011, *The Astrophysical Journal Supplement*, 193, 6
- Belczynski, K., Perna, R., Bulik, T., et al. 2006, *ApJ*, 648, 1110
- Beresnyak, A. 2012, *Phys Rev Lett*, 108, 35002
- Beresnyak, A., Jones, T. W., & Lazarian, A. 2009, *The Astrophysical Journal*, 707, 1541
- Blandford, R., & Eichler, D. 1987, *PHYSICS REPORTS V.154*, 154, 1
- Chertkov, M., Falkovich, G., Kolokolov, I., & Vergassola, M. 1999, *Phys. Rev. Lett.*, 83, 4065
- Eichler, D., Livio, M., Piran, T., & Schramm, D. N. 1989, *Nature*, 340, 126
- Etienne, Z. B., Liu, Y. T., Paschalidis, V., & Shapiro, S. L. 2012, *Physical Review D*, 85, 64029
- Federrath, C., Chabrier, G., Schober, J., et al. 2011, *Phys Rev Lett*, 107, 114504
- Freiburghaus, C., Rosswog, S., & Thielemann, F.-K. 1999, *The Astrophysical Journal Letters*, 525, L121
- Giacomazzo, B., Rezzolla, L., & Baiotti, L. 2011, *Physical Review D*, 83, 44014
- Hansen, B. M. S., & Lyutikov, M. 2001, *Monthly Notices of the Royal Astronomical Society*, 322, 695
- Haugen, N. E., Brandenburg, A., & Dobler, W. 2004, *Physical Review E*, 70, 16308
- Kazantsev, A. P. 1968, *Soviet Journal of Experimental and Theoretical Physics*, 26, 1031
- Li, L.-X., & Paczyński, B. 1998, *The Astrophysical Journal*, 507, L59
- Liu, Y. T., Shapiro, S. L., Etienne, Z. B., & Taniguchi, K. 2008, *Physical Review D*, 78, 24012
- Lyutikov, M., & Uzdensky, D. 2003, *ApJ*, 589, 893
- Metzger, B. D., & Berger, E. 2012, *The Astrophysical Journal*, 746, 48
- Metzger, B. D., Quataert, E., & Thompson, T. A. 2008, *Monthly Notices of the Royal Astronomical Society*, 385, 1455
- Metzger, B. D., Martínez-Pinedo, G., Darbha, S., et al. 2010, *Monthly Notices of the Royal Astronomical Society*, 406, 2650
- Mignone, A., Ugliano, M., & Bodo, G. 2009, *Monthly Notices of the Royal Astronomical Society*, 393, 1141
- Moffatt, H. 1978, Cambridge, England, Cambridge University Press, 1978. 353 p., -1,
- Nakar, E., & Piran, T. 2011, *Nature*, 478, 82
- Narayan, R., Paczynski, B., & Piran, T. 1992, *ApJ*, 395, L83
- Piran, T., Nakar, E., & Rosswog, S. 2013, 771
- Piro, A. L. 2012, arXiv, astro-ph.HE
- Ponty, Y., & Plunian, F. 2011, *Phys Rev Lett*, 106, 154502
- Price, D. J., & Rosswog, S. 2006, *Science*, 312, 719
- Rezzolla, L., Giacomazzo, B., Baiotti, L., et al. 2011, *The Astrophysical Journal Letters*, 732, L6
- Rhoads, J. E. 1997, *ApJ*, 487, L1
- Rosswog, S., Liebendörfer, M., Thielemann, F.-K., et al. 1999, *A&A*, 341, 499
- Schekochihin, A. A., Cowley, S. C., Hammett, G. W., Maron, J. L., & McWilliams, J. C. 2002, *New Journal of Physics*, 4, 84
- Schekochihin, A. A., Cowley, S. C., Taylor, S. F., Maron, J. L., & McWilliams, J. C. 2004, *The Astrophysical Journal*, 612, 276
- Shen, G., Horowitz, C. J., & Teige, S. 2010, *Phys. Rev. C*, 82, 015806
- Shen, H., Toki, H., Oyamatsu, K., & Sumiyoshi, K. 1998, *Progress of Theoretical Physics*, 100, 1013
- Thompson, C., & Duncan, R. 1993, *The Astrophysical Journal*, 408, 194
- Tobias, S. M., Cattaneo, F., & Boldyrev, S. 2011, eprint arXiv, 1103, 3138
- Tóth, G. 2002, *Journal of Computational Physics*, 180, 736
- Vainshtein, S. I., & Zel'dovich, Y. B. 1972, *Sov. Phys. Usp.*, 15, 159
- van Eerten, H. J., & MacFadyen, A. I. 2011, *ApJ*, 733, L37
- Zrake, J., & MacFadyen, A. 2012, *The Astrophysical Journal*, 744, 32
- Zrake, J., & MacFadyen, A. I. 2013, *The Astrophysical Journal Letters*, 763, L12